trans-Difluoroethylene Ozonide: Microwave Spectrum, Structure, Dipole Moment, ab Initio Calculations, and Anomeric Effect[1]

Marabeth S. LaBarge, Kurt W. Hillig II, Robert L. Kuczkowski,*

Department of Chemistry, The University of Michigan, Ann Arbor, Michigan 48109

and Dieter Cremer*

Lehrstuhl für Theoretische Chemie, Universität Köln, D-5000 Köln 41, Federal Republic of Germany
(Received: December 6, 1985)

The rotational spectra of six isotopic species of *trans*-difluoroethylene ozonide (*trans*-3,5-difluoro-1,2,4-trioxolane) were assigned. These included the parent species, the single- and double-substituted deuterium species, the double $^{18}O_p$, the triple ^{18}O, and the ^{13}C species. The spectrum consisted of *b*-type transitions with a 10:6 intensity alternation. The electric dipole moment was determined from Stark effect measurements to be $\mu_b = 0.994$ (5) D. These results support an average structure having an O_p–O_p twist ring conformation with C_2 symmetry and diaxial fluorine substituents. The shortening of the C–O_p bonds (1.368 Å) relative to the C–O_e bonds (1.401 Å) is very apparent in this member of the fluoroozonide series. Ab initio calculations were performed at the HF/6-31G* level and analyzed in terms of electron density distributions. Experimental and theoretical results are rationalized in terms of anomeric interactions with the peroxy oxygen atoms.

Introduction

Fluoroozonides have provided interesting insights on the anomeric effect in five-membered ring systems.[2-5] This effect refers to the preference of an electronegative substituent X (X = F, Cl, Br, N, OR, etc.) to adopt an axial orientation in heterocyclic rings.[6] Its origin is ascribed to the interaction between the oxygen π-type lone pair and the adjacent antibonding σ^* orbital of the C–X bond.[7] Although extensive experimental and theoretical investigations have been performed on carbohydrate structures, far less work has focused on five-membered ring systems outside the carbohydrate family.

Fluoroozonides are of particular interest since they offer both axial and equatorial substitution sites and potential interactions with ether (O_e) and peroxy oxygen (O_p) atoms. Evidence for the anomeric effect is demonstrated by the tendency for fluorine to be axial in fluoroethylene ozonide (FOz),[2] 1,1-difluoroethylene ozonide (1,1-F_2Oz),[3] and *cis*-difluoroethylene ozonide (*c*-F_2Oz).[4] To maximize the interaction with fluorine(s), the ozonide ring adjusts to maximize the overlap of the oxygen lone pairs and the σ^*_{CF} orbital.

In general, ozonides have provided much structural data for theoretical investigations. A series of ab initio calculations by Cremer have provided valuable information regarding the effects of substituents on the structural properties and reactivities of ozonides.[8] Most noteworthy was the recent calculation of the conformational potential of *c*-F_2Oz.[4] With the recent synthesis of *trans*-difluoroethylene ozonide (*t*-F_2Oz), the opportunity is presented to add insights from another interesting member of the ozonide family.

In this paper, we present the microwave structural data for *t*-F_2Oz and explore systematic trends in structural parameters of four members of the fluoroozonide series. Both spectroscopic measurements and ab initio calculations indicate that the anomeric effect stabilizes the structure and provides a reasonable explanation for the observed diaxial fluorines, C_2 ground-state symmetry, and the short C–O_p bond relative to C–O_e.

Experimental Section

Instrumentation. The microwave spectra were recorded with a Hewlett-Packard 8460A MRR spectrometer in the region of 18.0–40.0 GHz. The frequencies of the transitions for the d_1, $^{18}O_p$–$^{18}O_p$, and $^{18}O_3$ species were measured from chart recorder output to an accuracy of ±0.05 MHz. The microwave data for the normal, d_2, and ^{13}C species and Stark lobes for dipole moment measurements were collected with a PDP-11/23 computer interfaced to the spectrometer. By use of this signal-averaging technique, frequency measurements were typically accurate to ±0.02 MHz. For all measurements, the spectrometer cells were maintained between −40 and −60 °C with dry ice. The decomposition half-life of *t*-F_2Oz at these temperatures was typically 10–15 min in the gold-plated waveguide cell. Typical pressures used were 10–30 mTorr.

The enrichment of isotopically labeled *cis*-difluoroethylene and formyl fluoride was qualitatively analyzed by IR in the 4000–400-cm^{-1} range. Infrared spectra were recorded with a Perkin-Elmer 1330 grating spectrometer and a Nicolet 60SX Fourier transform spectrometer with a KBr beam splitter.

Theoretical Methods. The molecular orbital energies and one-electron density distribution $\rho(\mathbf{r})$ and associated Laplace field $\nabla^2\rho(\mathbf{r})$ were calculated at the Hartree–Fock level by employing Pople's 6-31G* basis set.[9] Calculations were made for the experimental geometry and an assumed model which had identical C–O_p and C–O_e bond distances.

Syntheses. The ozonolysis of *cis*-difluoroethylene (DFE) in $CClF_3$ at −95 °C produces *cis*- and *trans*-difluoroethylene ozonide.[10] In a previous paper the synthesis and purification of several isotopic species of both ozonides were reported.[4] The following enriched species were obtained from that work: *t*-F_2Oz-d_1 (~50% d_1, ~25% d_0, ~25% d_2) from ozonolysis of a 1:1 mixture of DFE and DFE-d_2; *t*-F_2Oz-d_2 from highly enriched DFE-d_2 (≥90%); $^{18}O_3$-enriched *t*-F_2Oz by direct reaction of DFE with 98% $^{18}O_3$

(1) Presented in part as paper TG4, 40th Symposium on Molecular Spectroscopy, The Ohio State University, Columbus, OH, 1985.
(2) Hillig, II, K. W.; Lattimer, R. P.; Kuczkowski, R. L. *J. Am. Chem. Soc.* **1982**, *104*, 988.
(3) Hillig, II, K. W.; Kuczkowski, R. L. *J. Phys. Chem.* **1982**, *86*, 1415.
(4) Hillig, II, K. W.; Kuczkowski, R. L.; Cremer, D. *J. Phys. Chem.* **1984**, *88*, 2025.
(5) Gillies, C. W.; Kuczkowski, R. L. *Isr. J. Chem.* **1983**, *23*, 446.
(6) (a) Lemieux, R. U. *Pure Appl. Chem.* **1971**, *25*, 527. (b) Eliel, E. L. *Angew. Chem., Int. Ed. Engl.* **1972**, *11*, 739. (c) Romers, C.; Altona, C.; Buys, H. R.; Havinga, E. *Top. Stereochem.* **1969**, *4*, 39.
(7) (a) Wolfe, S.; Whangbo, M. H.; Mitchell, D. J. *Carbohydr. Res.* **1979**, *69*, 1. (b) Szarek, W. A.; Horten, D., Eds. *Anomeric Effect, Origin and Consequences*; American Chemical Society: Washington, DC, 1979; ACS Symp. Ser. No. 87. (c) Lemieux, R. U. In *Molecular Rearrangements*; deMayo, P., Ed.; Interscience: New York, 1964.
(8) Cremer, D. *J. Am. Chem. Soc.* **1981**, *103*, (a) 3633, (b) 3619, (c) 3627; **1979**, *101*, (d) 7199. Cremer, D. *J. Chem. Phys.* **1979**, *70*, (e) 1898, (f) 1911, (g) 1928.
(9) Hariharan, P. C.; Pople, J. A. *Theor. Chim. Acta* **1973**, *28*, 213.
(10) Agopovich, J. W.; Gillies, C. W. *J. Am. Chem. Soc.* **1982**, *104*, 813. Gillies, C. W. *J. Am. Chem. Soc.* **1977**, *99*, 7239.

0022-3654/86/2090-3092$01.50/0

TABLE I: Assigned Rotational Transitions of the Normal Isotopic Species of *t*-F_2Oz

transition	ν(obsd)/MHz	ν(obsd) − ν(RR)[a]	ν(obsd) − ν(CD)[b]
3(3,1)–2(2,0)	32 605.04	−0.136	0.108
3(3,0)–2(2,1)	32 620.93	−0.136	0.011
5(2,4)–4(1,3)	31 859.93	−0.099	0.180
5(2,3)–4(1,4)	35 236.20	−0.101	0.033
6(4,3)–6(3,4)	27 582.80	−0.369	−0.068
6(4,2)–6(3,3)	27 539.92	−0.368	−0.018
7(2,6)–6(1,5)	38 890.37	−0.192	0.074
8(0,8)–7(1,7)	31 935.75	−0.150	0.018
8(1,8)–7(0,7)	34 259.78	−0.195	−0.028
9(0,9)–8(1,8)	36 273.27	−0.221	−0.090
9(1,9)–8(0,8)	37 959.09	−0.269	−0.082
9(1,8)–8(2,7)	32 167.02	−0.119	−0.050
10(1,9)–9(2,8)	37 344.00	−0.184	−0.057
12(5,8)–12(4,9)	35 203.55	−1.118	0.022
12(5,7)–12(4,8)	35 030.90	−1.107	0.066
16(1,15)–16(0,16)	30 164.90	0.465	−0.006
16(2,15)–16(1,16)	31 129.41	0.341	0.166
16(3,14)–16(2,15)	27 952.79	−0.415	−0.063
16(4,13)–16(3,14)	29 085.25	−1.050	−0.037
16(5,12)–16(4,13)	34 940.50	−1.596	−0.105
20(5,16)–20(4,17)	35 388.84	−2.174	−0.002
20(5,15)–20(4,16)	29 675.75	−2.294	−0.034
25(5,21)–25(4,22)	38,630.35	−2.700	−0.070
25(6,19)–25(5,20)	36 483.00	−4.400	0.009
28(6,22)–28(5,23)	32 136.37	−5.264	0.123
29(6,23)–29(5,24)	30 850.89	−5.410	−0.061
31(6,25)–31(5,26)	29 141.87	−5.343	−0.052
33(6,27)–33(5,28)	29 133.99	−4.741	−0.025
35(6,29)–35(5,30)	31 206.35	−3.658	−0.026
38(6,32)–38(5,33)	38 113.50	−1.665	0.110
42(8,34)–42(7,35)	38 645.48	−14.401	0.053
43(8,35)–43(7,36)	37 847.00	−13.622	0.103
46(8,38)–46(7,39)	38 801.00	−9.375	0.195

[a] Calculated from a rigid rotor fit of 178 transitions. [b] Calculated from a centrifugal distortion fit of 178 transitions.

in the ozone generator previously described;[2] $^{18}O_p$–$^{18}O_p$-enriched *t*-F_2Oz by insertion of unlabeled formyl fluoride in the ozonolysis of DFE with labeled ozone.

t-F_2Oz–^{13}C (~10% enrichment) was synthesized by insertion of ^{13}C-labeled formyl fluoride. The reaction mixture contained $H^{13}COF$ (14% ^{13}C) and DFE (90% DFE, 10% DFE-d_1) in CCl_2F_2. The ^{13}C-labeled formyl fluoride was prepared from $H^{13}COOH$ (40% ^{13}C) by the method of Olah and Kuhn.[11] Since DFE is not commercially available, it was made from a previously prepared sample of DFE-d_2 by exchange with 2 M $NaOH/H_2O$ at 128 °C and 15 atm in a stainless steel bomb for 72 h.[12] The enrichments of the d_1 and ^{13}C isotopic species were determined by microwave relative intensity measurements.

Results

Spectra. The microwave spectrum of the normal isotopic species consisted of moderately strong *b*-type transitions. In the region 26.5–40 GHz, several low-*J* R-branch transitions and numerous Q-branch transitions were assigned guided by Stark effects, intensities, and rigid rotor frequency fits. The Q-branch transitions belonged to K_{-1} series ranging from $1 \leftarrow 0$ to $8 \leftarrow 7$. The richness of the spectrum precluded the assignment of any vibrational satellites.

A centrifugal distortion fit for 178 transitions of the normal isotopic species was performed using our modified version of Kirchhoff's program CDIST.[13] The root-mean-square (rms) deviation of the quartic fit to three rotational constants and five linear combinations of τ's was 175 kHz. The agreement between observed and calculated transition frequencies for selected transitions of the normal species is given in Table I. Rotational constants are listed in Table II. The effects of centrifugal distortion are small in *t*-F_2Oz (relative to *c*-F_2Oz) with the largest deviation from a rigid rotor being only 15 MHz for $J = 42$.

TABLE II: Rotational Constants of Isotopic Species of *t*-F_2Oz[a]

species	*A*/MHz	*B*/MHz	*C*/MHz	no. of assigned transns
normal[b]	6093.333 (3)	2287.188 (1)	2001.709 (1)	178
d_2	5743.492 (7)	2206.778 (2)	1969.737 (2)	99
d_1	5913.052 (3)	2246.915 (14)	1985.702 (17)	16
$^{18}O_p$–$^{18}O_p$	5709.727 (5)	2265.447 (25)	1962.935 (26)	11
$^{18}O_3$	5562.080 (6)	2265.580 (15)	1945.249 (16)	17
^{13}C	6070.757 (12)	2274.544 (16)	1993.722 (6)	21

[a] Uncertainties in parentheses represent one standard deviation in the fit. [b] The centrifugal distortion constants (in kHz) for the normal species are $\tau_1 = -2.38$ (3), $\tau_2 = -0.552$ (10), $\tau_3 = 0.00$ (defined according to ref 13, eq 13), $\tau_{aaaa} = -7.64$ (16), $\tau_{bbbb} = -0.294$ (9), and $\tau_{cccc} = -0.348$ (7). The distortion constants for the d_2 and ^{13}C species are less accurate. They are given in the supplementary tables. The constants for the other three species are from rigid rotor fits.

TABLE III: Stark Coefficients[a] and Dipole Moment of *t*-F_2Oz

transition	*M*	$\Delta\nu/E^2$ obsd	$\Delta\nu/E^2$ calcd
3(2,2)–2(1,1)	1	−0.312 (2)	−0.313
4(3,1)–4(2,2)	3	−0.196 (2)	−0.195
	4	−0.305 (2)	−0.304
5(0,5)–4(1,4)	2	−0.155 (2)	−0.157
	3	−0.255 (3)	−0.255

$\mu_b = \mu_{total} = 0.994$ (5) D

[a] Stark coefficients ($\Delta\nu/E^2$) in units of 10^5 MHz/(V/cm)^2.

The assignment of the d_1, d_2, $^{18}O_p$–$^{18}O_p$, and $^{18}O_3$ isotopic species presented no difficulties since they were rather highly enriched. A centrifugal distortion analysis was performed for the d_2 and ^{13}C species. Rigid rotor fits were employed for the other species. The fits had typical rms deviations of 80 kHz. The rotational constants for the six isotopic species are given in Table II. A complete list of the assigned transitions of all the isotopic species is available (Tables S1–S6, supplementary material).

The spectrum of the ^{13}C species was predicted by a weighted least-squares fit of the moments of inertia of the other five isotopic species and assumed structural parameters[14] using the procedure known as "predicate observables" or "diagnostic least squares".[15] This predicted a 20-MHz spectral range to search for selected ^{13}C transitions. Within the 20-MHz window many candidates were observed. Although the strength of the normal isotopic spectrum suggested that the ^{13}C species should be observable in natural abundance (2%), an unambiguous assignment could not be made. After synthesis of *t*-F_2Oz–^{13}C, a comparison between spectra from unenriched and enriched ^{13}C samples allowed a facile assignment to be made. It was accomplished by first identifying the ($J'_{4,K'} \leftarrow J''_{3,K''}$) *Q*-branch series $J \geq 8$. This series of lines with alternating symmetry displayed nearly equivalent intensities consistent with the absence of C_2 symmetry upon isotopic substitution. The experimental rotational constants agreed within 100 kHz of those from the predicate observables calculations, exemplifying the utility of this method in searching for isotopic species.

Nuclear Spin Effects. Intensity alternations in rotational levels of opposite symmetry for Q-branch and R-branch *K*-doublet pairs were observed for the normal, d_2, $^{18}O_3$, and $^{18}O_p$–$^{18}O_p$ isotopic species but were absent in the d_1 and ^{13}C spectra. The observed ratio for the 3(3,0)–2(2,1) and 3(3,1)–2(2,0) transitions in the

(11) Olah, G. A.; Kuhn, S. J. *J. Am. Chem. Soc.* **1960**, *82*, 2380.
(12) Craig, N. C.; Overend, J. *J. Chem. Phys.* **1969**, *51*, 1127.
(13) Kirchhoff, W. H. *J. Mol. Spectrosc.* **1972**, *41*, 333.
(14) Structural calculations were performed with our extended version of Schwendeman's STRFIT program: Schwendeman, R. H. In *Critical Evaluation of Chemical and Physical Structural Information*; Lide, D. R., Paul, M. A., Eds.; National Academy of Sciences: Washington, DC, 1974; pp 74–115.
(15) Bartell, L. S.; Romanesko, D.; Wong, T. C. *Spec. Period. Rep.: Mol. Struct. Diffr. Methods* **1975**, *3*, Chapter 4. See also: Nösberger, P.; Bauder, A.; Günthard, Hs. H. *Chem. Phys.* **1973**, *1*, 418. Kierns, J. J.; Curl, Jr., R. F. *J. Chem. Phys.* **1968**, *48*, 3773.

TABLE IV: Principal Axis Coordinates (Å) in t-F_2Oz

coordinate	r_0	r_s	coordinate	r_0	r_s
$\pm a$ (H)	1.3099	1.3083[a,b]	$\pm a$ (O_e)	0.0	0.0
b (H)	−0.5272	−0.5336[a]	b (O_e)	−1.0549	−1.0569[d]
$\pm c$ (H)	1.5117	1.5091[a]	$\pm c$ (O_e)	0.0	0.0
$\pm a$ (C)	0.9853	0.9845[a]	$\pm a$ (F)	2.0677	2.0677[e]
b (C)	−0.1985	−0.2144[a]	b (F)	−0.2820	−0.2711
$\pm c$ (C)	0.5228	0.5158[a]	$\pm c$ (F)	0.3112	0.3101
$\pm a$ (O_p)	0.4343	0.4359[c]			
b (O_p)	1.0445	1.0442[c]			
$\pm c$ (O_p)	0.5828	0.5823[c]			

[a] Kraitchman single substitution. [b] Double substitution coordinates were 1.3101, 0.5272, and 1.5113 Å. [c] Chutjian–Nygaard double substitution. [d] Single substitution using $^{18}O_3$, $^{18}O_p$–$^{18}O_p$, and center of mass shift to normal isotopic species. See structure section in text. [e] From least-squares fit of inertial equations described in text.

TABLE V: Ring Structural Parameters of t-F_2Oz from Coordinates in Table IV

parameter[a]	r_0	r_s	parameter[a]	r_0	r_s
C–O_e	1.406	1.395	∠C–O–C	105.0	105.0
C–O_p	1.361	1.375	∠O–C–O	106.8	106.8
O_p–O_p	1.454	1.455	∠C–O–O	101.9	101.9
C–F	1.369	1.363	∠O_p–C–F	113.7	113.7
C–H	1.092	1.093	∠O_e–C–F	106.9	106.9
τ(C–O–O–C)	42.0	41.7			
τ(O–O–C–F)	83.6	84.6			

[a] Bond distances in angstroms and bond angles in degrees.

normal isotope was 0.62 ± 0.02. This result is consistent with the 6:10 ratio of nuclear spin weights expected for a molecule with C_2 symmetry following Bose–Einstein statistics. A 6:10 ratio was also measured for several transitions of the triple- and double-substituted ^{18}O isotopes. The intensities in the d_2 spectrum where Fermi–Dirac statistics apply were consistent with the expected value of 7/5.

Dipole Moment. The second-order Stark coefficients for five M components of three transitions are listed in Table III. Each value of $\Delta\nu/E^2$ is the average of measurements for 10 electric fields. The electric field was calibrated on the $J = 2 \leftarrow 1$, $M = |1|$ transition of OCS at 24 325.928 MHz.[16] A least-squares fit to μ_b^2 gave $\mu_b = 0.994$ (5) D. A fit to the square of all three dipole components gave values of μ_a and $\mu_c < 0.01$ D.

Structure. Evidence from nuclear spin statistics and from the dipole moment directed along the b inertial axis supports C_2 symmetry for t-F_2Oz. With C_2 symmetry 13 coordinates must be determined to define the molecular structure. If one utilizes the first moment ($\sum m_i b_i$) and product conditions ($\sum m_i a_i c_i$), at least 11 independent experimental inertial constants are required to determine the structure. Using our extended version of the program STRFIT,[14] we calculated the coordinates and structure by several different methods.

The r_0 coordinates in Table IV were calculated from a least-squares fit to 20 inertial parameters of the parent and isotopic species. The quality of the fit was excellent as indicated by the rms deviation of 0.004 amu Å^2 between observed and calculated moments. The largest difference between observed and calculated moments was 0.008 amu Å^2 for I_b of the $^{18}O_p$–$^{18}O_p$ species. The r_0 structural parameters are listed in Table V.[17]

Kraitchman[18] and Chutjian–Nygaard[19] calculations were also performed to determine the substitution (r_s) coordinates of the H, O_p, and C atoms. The b_s coordinate of O_e was also calculated by using the $^{18}O_3$ and $^{18}O_p$–$^{18}O_p$ data followed by a center of mass transposition back to the principal axis system of the normal isotopic species. As seen from Table IV, there is reasonable agreement between the r_0 and r_s coordinates confirming the C_2 symmetry of the molecule. The largest difference is in the b coordinate of the carbon atom (0.0159 Å). This may result since Kraitchman's equations often underestimate a coordinate at a site approaching an inertial plane.[14,20,21] Using these r_s coordinates, we obtained the fluorine positions in Table IV from a least-squares fit to $\sum m_i b_i$, $\sum m_i a_i c_i$, and the three equations $P_{aa} = \sum m_i a_i^2$ etc. The "mixed r_0 and r_s" structure determined from these coordinates is given in Table V. The r_0 and partial r_s structures agree well except for the differences of 0.010–0.015 Å for the C–O_p and C–O_e bond lengths.

TABLE VI: Structural Parameters of t-F_2Oz[a]

bond		angle		dihedral angle	
C–O_e	1.401 (10)	C–O_e–C	105.3 (3)	C–O_p–O_p–C	41.9
C–O_p	1.368 (10)	O_e–C–O_p	106.8 (2)	O_e–C–O_p–O_p	−34.0
O_p–O_p	1.455 (1)	C–O_p–O_p	101.8 (2)	C–O_e–C–O_p	13.8
C–F	1.366 (3)	O_e–C–F	107.5 (7)	C–O_e–C–F	−108.0
C–H	1.093 (1)	O_e–C–H	111.6 (4)	C–O_e–C–H	134.6
		O_p–C–F	113.2 (6)	O_p–O_p–C–F	84.1
		O_p–C–H	110.2 (6)	O_p–O_p–C–H	−155.5
		F–C–H	107.5 (2)		

[a] The average of the results in Table V with uncertainties sufficient to encompass both calculations. Bond distances in angstroms and bond angles in degrees.

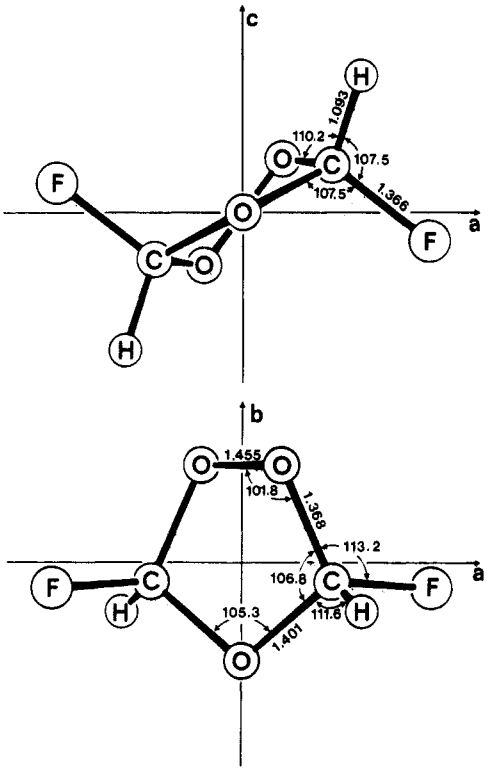

Figure 1. *trans*-Difluoroethylene ozonide: projection on to *ac* plane (top), projection on *ab* plane (bottom).

Consideration of the differences between the parameters computed by the two methods has prompted us to report the average of these values (Table VI) with uncertainty ranges that encompass both calculations as the most reliable structure for t-F_2Oz. This choice is made since both methods have relative merits. The r_0 method samples the moments of inertia of all the isotopes to obtain the coordinates and hence is probably more reliable in determining the carbon b coordinate. However, the accuracy of the r_0 structure (i.e., extent of vibration–rotation interactions) cannot be determined without a vibrational analysis. The attractiveness of the r_s method lies in the fact that the ring parameters are effectively

(16) Muenter, J. S. *J. Chem. Phys.* **1968**, *48*, 4544.
(17) Conversion factor AI_s = 505379.05 MHz amu Å^2.
(18) Kraitchman, J. *Am. J. Phys.* **1953**, *21*, 17.
(19) Nygaard, L. *J. Mol. Spectrosc.* **1976**, *62*, 292. Chutjian, A. *Ibid.* **1964**, *14*, 361.
(20) Harmony, M. D.; Laurie, V. W.; Kuczkowski, R. L.; Schwendeman, R. H.; Ramsay, D. A.; Lovas, F. J.; Lafferty, W. J.; Maki, A. J. *J. Phys. Chem. Ref. Data* **1979**, *8*, 619.
(21) Costain, C. C. *J. Chem. Phys.* **1958**, *29*, 864.

TABLE VII: Comparison of Ozonide Structures

parameter[a]	EtOz[b]	*t*-F_2Oz[d]	FOz[e]	*c*-F_2Oz[f]	1,1-F_2Oz[g]
C_F–O_e	1.415	1.401	1.382	1.385	1.368
C_F–O_p	1.410	1.368	1.382	1.376	1.360
O_p–O_p	1.461	1.455	1.463	1.468	1.467
C–F_{ax}		1.366	1.375	1.376	1.359
∠C–O_e–C	104.6	105.3	105.3	105.3	103.9
∠O_e–C–O_p	105.7	106.8	107.6	107.4	110.5
∠C–O_p–O_p	99.2	101.8	101.1	105.5	101.8
τ(C–O_p–O_p–C)	49.4	41.9	46.0	0	42
τ(F–C–O_p–O_p)		84.1	83.5	100.7	96
phase angle, ϕ[c]	90	90	97.0	180	113.0
puckering amplitude, q[c]	0.456	0.376	0.431	0.263	0.424

[a] Bond distances in angstroms and bond angles in degrees. [b] $C_F = C_H$. [c] For a definition of ϕ and q, see: Cremer, D.; Pople, J. A. *J. Am. Chem. Soc.* **1975**, *97*, 1354. [d] This work. [e] Reference 2. [f] Reference 4. [g] Reference 3.

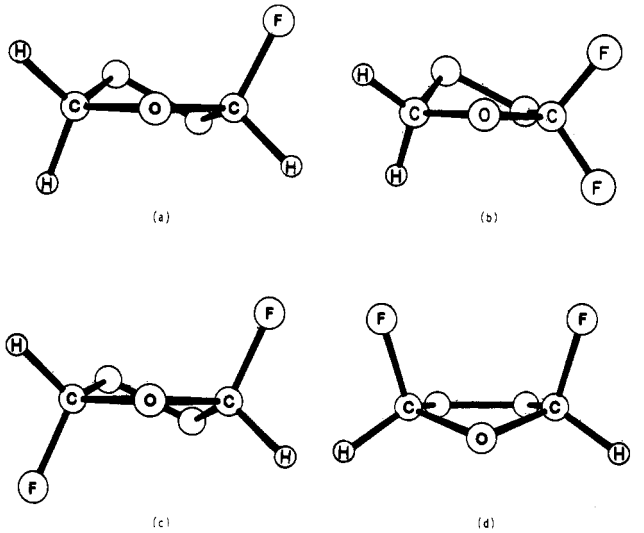

Figure 2. Conformations of fluoroozonides: (a) fluoroethylene ozonide (FOz), (b) 1,1-difluoroethylene ozonide (1,1-F_2Oz), (c) *trans*-diluoroethylene ozonide (*t*-F_2Oz), (d) *cis*-difluoroethylene ozonide (*c*-F_2Oz).

determined without relying on the center of mass or product of inertia conditions, thereby reducing vibrational effects. While most of the oxygen and carbon coordinates which define the ring are not small, the carbon *b* coordinate (~0.2 Å) is marginal enough to reduce confidence in this approach. Although the physical relevance of the preferred structure in Table VII is no longer clear, it seems likely that the structural parameters and uncertainties encompass the equilibrium structure. The structure of *t*-F_2Oz is shown in Figure 1.

Discussion

Structure. The diversity among the fluoroozonide conformations is apparent in Figure 2.[22] The conformation of *t*-F_2Oz, like the prototype ethylene ozonide (EtOz), is described as an O_p–O_p twist with C_2 symmetry. FOz has a distorted conformation falling between the twist and peroxy envelope while 1,1-F_2Oz has an O_H envelope conformation. The most unusual structure is that of *c*-F_2Oz, which has an O_e envelope conformation and C_s symmetry. These various conformations are due to an interplay of ring–substituent, substituent–substituent, and puckering forces.[4] The tendency of F substituents to act as σ-acceptors and π-donors favors their placement in axial positions. In this orientation, the σ^*_{CF} orbital is suitably arranged to interact with O_e and O_p lone-pair orbitals via an anomeric interaction.[6,7]

A comparison of the structural parameters for this series is given in Table VII and also shows the influence of the anomeric effect. One characteristic in this series is the relatively long C–F bond. As discussed recently,[3] this parameter is about 0.03–0.04 Å longer than expected based on a simple inductive model. In a similar vein, the C_F–O bonds are shorter than those found in ozonides without fluorine substituents where values of 1.415–1.425 Å have been found. This lengthening and shortening, respectively, are consistent with oxygen lone-pair delocalization into the σ^*_{CF} orbital in accordance with the anomeric effect.

A most interesting feature in *t*-F_2Oz is the difference in the C–O_p bond (1.368 Å) relative to the C–O_e bond (1.401 Å). Such a pronounced difference was not so apparent in the other members of the fluoroozonide series. It suggests that the O_p electron lone pair interacts more strongly than the O_e lone pair with the C–F group.

In order to provide additional insight on the anomeric interactions in *t*-F_2Oz, ab initio calculations for a geometry very close to the experimentally derived r_0 geometry were analyzed (Table VIII, experimental geometry). Examination of the possible interactions between the two highest occupied ring MO's (they are essentially lone-pair orbitals; see ref 8g, Figure 3) and the S and A combinations of σ^*_{CF} provides some evidence that the anomeric

(22) For a general overview of earlier substituted ozonide conformations, see: Kuczkowski, R. L. *Acc. Chem. Res.* **1983**, *16*, 42.

TABLE VIII: Positions of Ether and Peroxy Oxygen Lone Pairs (lp) of *t*-F_2Oz

parameter[a]	exptl geometry[b]	assumed geometry[b]
lp_{10}–O_1–lp_{11}	140.9	142.3
lp_{12}–O_3–lp_{13}	149.8	151.2
lp_{12}–O_3–O_4–lp_{14}	108.7	112.4
lp_{13}–O_3–O_4–lp_{14}	45.6	43.5
lp_{13}–O_3–O_4–lp_{15}	160.1	160.7
lp_{10}–O_1–C_2–F_6	146.9	146.7
lp_{11}–O_1–C_2–F_6	1.6	3.0
Δ[c]	17.4	18.2
lp_{12}–O_3–C_2–F_6	17.3	16.0
lp_{13}–O_3–C_2–F_6	176.1	175.4
Δ[c]	10.5	10.3
abs energy[d]	−500.25702	−500.25245
rel energy[e]	0	2.9

[a] See Figure 3 for numbering of lp and atoms. [b] Essentially r_0 in Table V except that O_1–C_2 = O_3–C_2 = 1.406 Å in the assumed geometry. Other dihedral angles of interest, in the order τ, experimental, assumed, are as follows: τ(F_6–C_2–O_3–O_4), 83.7°, 84.5°; τ(F_6–C_2–O_1–C_5), 108.2°, 109.0°; τ(H_7–C_2–O_3–O_4), 155.2°, 155.4°; τ(H_7–C_2–O_1–C_5), 134.8°, 134.9°. [c] Mean deviation of lp_{10} and lp_{11} (or lp_{12} and lp_{13}) from a parallel alignment with C–F bond. [d] HF/6-31G* values (in hartree). [e] In units of kcal/mol.

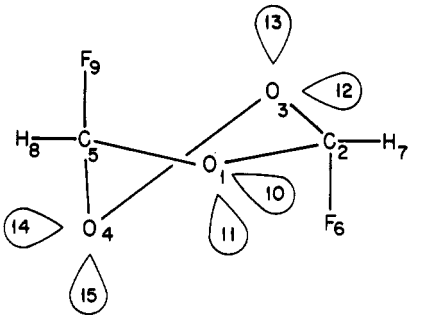

Figure 3. Atom and lone-pair (lp) numbering. See Tables XIII and IX.

TABLE IX: Electron Lone-Pair Concentrations at the Ether (O_1) and Peroxy (O_3) Oxygen Atoms of t-F_2Oz in Terms of $\rho(\mathbf{r})$ and the Laplace Distribution $-\nabla^2\rho(\mathbf{r})$

	exptl geometry		assumed geometry	
parameter[a]	$-\nabla^2\rho(\mathbf{r})$[b]	$\rho(\mathbf{r})$[c]	$-\nabla^2\rho(\mathbf{r})$[b]	$\rho(\mathbf{r})$[c]
O_1 lp_{10}	161.4	6.720	162.3	6.733
O_1 lp_{11}	161.4	6.720	162.3	6.733
O_3 lp_{12}	196.2	7.179	198.4	7.196
O_3 lp_{13}	198.9	7.233	201.2	7.250

[a] Atoms and lone pairs numerically defined in Figure 3. [b] In units of e/Å^5. [c] In units of e/Å^3.

effect involving O_p lone pairs is possibly stronger than the one involving O_e lone pairs. It is difficult to extract these orbitals from the calculated MO's since in the three-dimensional structure p_x, p_y, and p_z mix. In order to base the discussion on molecular properties which provide a better description of anomeric interactions, the total one-electron density distribution $\rho(\mathbf{r})$ and its associated Laplace field $\nabla^2\rho(\mathbf{r})$ were investigated. The analysis of $\rho(\mathbf{r})$ has provided reasonable descriptions of covalent bonding in hydrocarbon C–C bonds,[23] homoaromatic systems,[24] three-membered rings,[25] and numerous substituted cyclopropanes[26] in terms of empirical bonding concepts familiar to chemists, i.e., bond order and π-character. The latter is determined by the ellipticity ϵ at the bond critical point $\mathbf{r}_b$.[23,25,27] Information about bonding obtained from the properties of $\rho(\mathbf{r})$ can be substantiated when determining the stationary points of $\nabla^2\rho(\mathbf{r})$.[28,29] The latter provides evidence where electrons concentrate ($\nabla^2\rho(\mathbf{r}) < 0$) and where electrons are depleted ($\nabla^2\rho(\mathbf{r}) > 0$). Concentration lumps are found in the bonding and in the lone-pair regions. One can consider these concentration lumps to arise from bonding and electron lone pairs.[25,26] In the following analysis, the position of maximum concentration in the lone-pair region will be called the "position" of the electron lone pair (lp).

Investigation of the calculated $\rho(\mathbf{r})$ and $\nabla^2\rho(\mathbf{r})$ distributions of t-F_2Oz suggests that the driving force for the shortening of C–O_p relative to C–O_e is a result of lone pair–lone pair repulsion between adjacent O_p atoms which makes the peroxy group a stronger π-donor than the ether oxygen. The degree of π-donation into the σ^*_{CF} orbital determines the length of the C–O_p bond.

In Table VIII the positions of the oxygen lone pairs are identified. There are two pairs at each O atom. At the two peroxy oxygens one lone pair is in the axial position and the other is in the equatorial position. These lone pairs are largely staggered as revealed by the dihedral angles (lp–O_3–O_4–lp) of 46°, 160°, and 109°.

There is a significant difference between the ether and peroxy lone pairs. The peroxy lone pairs are clearly more concentrated and represent a higher electron density as seen by the values of $\rho(\mathbf{r})$ and $\nabla^2\rho(\mathbf{r})$ in Table IX. This means that O_3 and O_4 should be stronger π-donors than O_1.

Both O_3 (O_4) and O_1 lone pairs are almost parallel to the σ^*_{CF} bond, which is a prerequisite for an anomeric effect. On the average, however, the peroxy lone pairs are 7° closer to a parallel alignment with the C–F bond. (Consideration of the dihedral angles given in Table VIII reveals that the C–F bond is more nearly perpendicular to C–O–O than C–O–C. Hence, the C–F bond is in the right orientation for interaction with the 2p π-orbitals of O_3.) This is related to the fact that the lp-O–lp angle widens from 141° to 150° when going from the ether to the peroxy group. Obviously, lp's at O_3 and O_4 try to interact more strongly with the substituent. The result is a delocalization of electrons into bonds O_3–C_2 and O_4–C_5. The electron density at the bond critical point $\mathbf{r}_b$ of O_3–C_2 is higher than that at $\mathbf{r}_b$ of O_1–C_2. Accordingly, the O_3–C_2 bond order exceeds that of the bond O_1–C_2 by 0.3 (1.58 vs. 1.28; see Table X). Also, the effective ellipticity (ϵ) of the former bond is higher than that of the latter. This is indicative of increased π-character in the O_3–C_2 bond.[23]

In order to substantiate these arguments, the value of the O_3–C_2 bond length was lengthened to the value of the O_1–C_2 bond (assumed geometry, Table VIII). As a result, the total energy increased by 2.9 kcal/mol. The lp concentrations at O_3 and O_4 also increase when lengthening the adjacent C–O bond (Table IX). However, the corresponding bond order as well as the effective ellipticity (Table X) is still somewhat larger than that of the O_1–C_2 bond although the two bond lengths are equal. These trends are indicative of a strong anomeric effect between O_3 (O_4) and the C–F bonds.

In conclusion, the structural trends in the fluoroozonides can be rationalized in terms of the anomeric effect. The bond lengths and angles in t-F_2Oz are consistent with those of the other members of the series except for the greater anomeric shortening of the C–O_p bond. The values of ρ_b, $\nabla^2\rho(\mathbf{r})$, and effective ellipticity enable this interaction to be quantified in terms of the charge distribution which complements the qualitative description in terms of orbital interactions.

Dipole Components. The observed dipole components of EtOz, FOz, 1,1-F_2Oz, and t-F_2Oz can be reproduced reasonably well by vectorially summing the C–F, C–O_p, C–O_e, and C–H bond moments. The bond moments were determined by fitting seven of the eight observed dipole components and the corresponding structures of these ozonides. The results of the least-squares fit and derived bond moments are given in Table XI. There is relatively good agreement (≤6%) between the observed and calculated molecular dipole components except for μ_c of FOz which

TABLE X: Bond Order, Ellipticity, and $\rho(\mathbf{r})$ at Bond Critical Point $\mathbf{r}_b$ of t-F_2Oz

	exptl geometry		assumed geometry	
parameter[a]	O_1–C_2	O_3–C_2	O_1–C_2	O_3–C_2
ρ_b[b]	1.892	2.066	1.891	1.910
bond order	1.28	1.58	1.28	1.31
ϵ_{eff}	0.431	0.719	0.437	0.484

[a] For definition of parameters, see Table III of ref 25. [b] In units of e/Å^3.

TABLE XI: Bond Moments Derived from Dipole Components in Ozonides

molecule	dipole component	obsd[f]	calcd[f]
EtOz[a]	μ_a	1.09 (1)	1.04
FOz[b]	μ_a	1.456 (7)	1.379
	μ_b	−1.346 (34)	−1.275
	μ_c	−1.199 (13)	(−1.980)[e]
1,1-F_2Oz[c]	μ_a	2.20 (1)	2.25
	μ_b	−1.50 (9)	−1.59
	μ_c	−0.65 (18)	−0.61
t-F_2Oz[d]	μ_b	0.995 (4)	1.02

C–F moment = 1.83 D
C–O_p moment = 1.72 D
C–O_e moment = 1.81 D
H–C moment = 0.44 D

[a] Gillies, C. W.; Kuczkowski, R. L. *J. Am. Chem. Soc.* **1972**, *94*, 6337. [b] Reference 2. [c] Reference 3. [d] This work. [e] Dipole component not included in fit. [f] In Debyes.

(23) Bader, R. F. W.; Slee, T. S.; Cremer, D.; Kraka, E. *J. Am. Chem. Soc.* **1983**, *105*, 5061.
(24) Cremer, D.; Kraka, E.; Slee, T. S.; Bader, R. F. W.; Lau, C. D. H.; Nguyen-Dang, T. T.; MacDougall, P. S. *J. Am. Chem. Soc.* **1983**, *105*, 5069.
(25) Cremer, D.; Kraka, E. *J. Am. Chem. Soc.* **1985**, *107*, 3800. Table III lists the definitions of the parameters used to analyze energy and electron density.
(26) Cremer, D.; Kraka, E. *J. Am. Chem. Soc.* **1985**, *107*, 3811.
(27) The bond critical point $\mathbf{r}_b$ corresponds to the minimum of $\rho(\mathbf{r})$ along the path of maximum electron density connecting two atomic nuclei; i.e., $\mathbf{r}_b$ is a saddle point of $\rho(\mathbf{r})$ in three dimensions. There exists no path of maximum electron density and, hence, no bond critical point between those atoms of a molecule which are not bonded. The properties of $\rho(\mathbf{r}_b)$ can be used to characterize the corresponding bond. See ref 23 and 26.
(28) Cremer, D.; Kraka, E. *Croat. Chem. Acta* **1984**, *57*, 1259 and references cited therein.
(29) (a) Bader, R. F. W.; McDougall, P. J.; Lau, C. D. H. *J. Am. Chem. Soc.* **1984**, *106*, 1594. (b) Bader, R. F. W.; Essén, H. *J. Chem. Phys.* **1984**, *80*, 1943.

was not included in the fit. This result is somewhat anomalous and presently cannot be explained. In general, the observed transferability of the four bond moments among the members of the fluoroozonide series has potential usefulness for predicting the dipole moment for new members of the series.

Acknowledgment. This work was supported by Grants CHE-8005471 and CHE-8303615 from the National Science Foundation. Support at the Universität Köln was provided by the Deutsche Forschungsgemeinschaft and the Fond der Chemischen Industrie. All ab initio calculations were carried out at the Rechnenzentrum der Universität Köln.

Registry No. *t*-F_2Oz, 54892-65-8; *t*-F_2Oz-d_2, 102307-21-1; *t*-F_2Oz-d_1, 102307-22-2; *t*-F_2Oz-^{18}Op-^{18}Op, 102342-10-9; *t*-F_2Oz-$^{18}O_3$, 102307-23-3; *t*-F_2Oz-^{13}C, 102307-24-4; DFE, 1630-77-9.

Supplementary Material Available: Tables S1-S6 listing transition frequencies for the ground vibrational states of the normal and isotopic species (10 pages). Ordering information is given on any current masthead page.

A Theory of Vibrational Transition Frequency Shifts Due to Hydrogen Bonding

Shi-yi Liu and Clifford E. Dykstra*

Department of Chemistry, University of Illinois, Urbana, Illinois 61801 *(Received: January 3, 1986)*

Changes in vibrational transition frequencies, usually red shifts, are characteristic of the effects of hydrogen bonding. A theory based on intermolecular electrical interaction has been developed and tested to explain these shifts entirely from monomer properties. Dipole and quadrupole polarizabilities and permanent electrical moments through the octupole give rise to important changes in a molecule's stretching potential when it interacts with the electrical field of another molecule. This interaction potential tends to be almost linear with the stretching coordinate, and so a change in the vibrational transition frequency arises largely because of the intrinsic anharmonicity of the original, or unperturbed stretching potential. Knowledge of the interaction potential, which we show can be obtained from a simple electrical model, and knowledge of the vibrational anharmonicity parameters are then sufficient to adequately account for vibrational shifts. Furthermore, because the interaction potential function prescribes a new equilibrium bond length, the usual correlation between bond length changes and vibrational frequency changes is obtained as a more quantitative relation involving the intrinsic anharmonicity and the slope of the interaction potential. Calculations on a number of hydrogen-bonded complexes of hydrogen fluoride show very good agreement with experiment.

Introduction

One of the significant advances in contemporary chemical physics has been the capability to study weakly bound complexes in virtually as much detail as the molecules that make up such complexes. From there being all too infrequent papers on the subject a decade and a half ago, there is now a wealth of information on structures, stabilities, vibrational frequencies, and the dynamics of van der Waals and hydrogen-bonded complexes, including many dimers, some trimers, and even large aggregates. Techniques utilizing molecular beam electric resonance,[1-4] pulsed beam microwave spectroscopy,[5-7] vibrational predissociation,[8,9] matrix isolation,[10,11] long-path-length absorption,[12-15] and laser-induced fluorescence[16] have all played a role in this direct attack on a problem that is fundamental in molecular science. What is particularly exciting is the prospect of this new information being used to aid the refinement of hydrogen-bonding interaction potentials in molecular dynamics simulations of biomolecules or large molecular clusters that serve as models of condensed-phase systems.

Beginning with Coulson's partitioning of the hydrogen bond strength in the water dimer,[17] hydrogen bonding has been thought of as arising from a number of competing effects. These include electrostatic interaction of the permanent electrical moments of interacting species, polarization of charge, dispersion, charge transfer, and exchange effects. Morokuma developed some of the first calculational means for partitioning energies obtained from ab initio electronic structure wave functions[18-20] among such effects. Partitioning methods were also formulated by Kollman,[21-24] and one recurring conclusion of such analyses is that electrostatic interactions have a significant role in hydrogen bonding.

The possible range of hydrogen bond strengths is unquestionably large. At one end are charged complexes such as FHF^- where the hydrogen bond strength is 39 kcal[25,26] and the proton is symmetrically located between the two bonding partners. This type of bonding, though, is easily understood in terms of usual chem-

(1) Dyke, T. R.; Howard, B. J.; Klemperer, W. *J. Chem. Phys.* **1972**, *56*, 2442.
(2) Novick, S. E.; Davies, P.; Harris, S. J.; Klemperer, W. *J. Chem. Phys.* **1973**, *59*, 2273.
(3) Dyke, T. R.; Muenter, J. S. *J. Chem. Phys.* **1974**, *60*, 2929.
(4) Klemperer, W. *J. Mol. Struct.* **1980**, *59*, 161.
(5) Balle, T. J.; Campbell, E. J.; Keenan, M. R.; Flygare, W. H. *J. Chem. Phys.* **1979**, *71*, 2723. **1980**, *72*, 922.
(6) Balle, T. J.; Flygare, W. H. *Rev. Sci. Instrum.* **1981**, *52*, 33.
(7) Campbell, E. J.; Read, W. G.; Shea, J. A. *Chem. Phys. Lett.* **1983**, *94*, 69.
(8) Lisy, J. M.; Tramer, A.; Vernon, M. F.; Lee, Y. T. *J. Chem. Phys.* **1981**, *75*, 4733.
(9) Cassasa, M. P.; Western, C. M.; Cellii, F. G.; Brinza, D. E.; Janda, K. C *J. Chem. Phys.* **1983**, *79*, 3227.
(10) Johnson, G. L.; Andrews, L. *J. Am. Chem. Soc.* **1982**, *104*, 3043.
(11) Andrews, L. *J. Phys. Chem.* **1984**, *88*, 2940.
(12) Thomas, R. K. *Proc. R. Soc. London, Ser. A* **1971**, *A325*, 133.
(13) Pine, A. S.; Lafferty, W. J. *J. Chem. Phys.* **1983**, *78*, 2154.
(14) Pine, A. S.; Lafferty, W. J.; Howard, B. J. *J. Chem. Phys.* **1984**, *81*, 2939.
(15) Kyrö, E. K.; Shoja-Chaghervand, P.; McMillan, K.; Eliades, M.; Danzeiser, D.; Bevan, J. W. *J. Chem. Phys.* **1983**, *79*, 78.
(16) Levy, D. H. *Adv. Chem. Phys.* **1980**, *31*, 197.
(17) Coulson, C. A. *Research* **1957**, *10*, 149.
(18) Kitaura, K.; Morokuma, K. *Int. J. Quantum Chem.* **1976**, *10*, 325.
(19) Umeyama, H.; Morokuma, K. *J. Am. Soc.* **1977**, *99*, 1316.
(20) Morokuma, K. *Acc. Chem. Res.* **1977**, *10*, 294.
(21) Kollman, P. A.; Allen, L. C. *Chem. Rev.* **1972**, *72*, 283.
(22) Kollman, P. A. *J. Am. Chem. Soc.* **1977**, *99*, 4875.
(23) Kollman, P. A. Ed.; In *Applications of Electronic Structure Theory*, Schaefer, H. F., Plenum: New York, 1977.
(24) Singh, V. C.; Kollman, P. A. *J. Chem. Phys.* **1984**, *80*, 353.
(25) Harrel, S. A.; McDaniel, D. H. *J. Am. Soc.* **1964**, *86*, 4497.
(26) Larson, J. W.; McMahon, T. B. *J. Am. Chem. Soc.* **1982**, *104*, 5848.

0022-3654/86/2090-3097$01.50/0